Application of sphere-cylinder scattering model to skeletal muscle

Honghui He,[1,2] Nan Zeng,[1] Ran Liao,[1] Tianliang Yun,[1,2] Wei Li,[1,2] Yonghong He,[1] and Hui Ma[1,2,*]

[1]*Laboratory of Optical Imaging and Sensing, Graduate School at Shenzhen, Tsinghua University, Shenzhen 518055 China*

[2]*Key Laboratory for Molecular and Nanosciences of Education Ministry, Department of Physics, Tsinghua University, Beijing 100084 China*

**mahui@tsinghua.edu.cn*

Abstract: By comparing the spatially resolved unpolarized, polarized reflectance and Mueller matrix elements of skeletal muscle with a scattering medium containing polystyrene microspheres and silk fibers, we demonstrate that the sphere-cylinder scattering model (SCSM) can reproduce the characteristic features of skeletal muscle. Both experiments and polarization sensitive Monte Carlo simulation provide evidences that SCSM may be used to characterize the structural and optical properties of skeletal muscle.

OCIS codes: (170.3660) Light propagation in tissues; (290.5855) Scattering, polarization

References and links

1. K. S. Saladin, *Anatomy and Physiology* (Watnick, New York, 2010).
2. A. F. Huxley, and R. Niedergerke, "Measurement of the striations of isolated muscle fibres with the interference microscope," J. Physiol. **144**(3), 403–425 (1958).
3. R. Rüdel, and F. Zite-Ferenczy, "Interpretation of light diffraction by cross-striated muscle as Bragg reflexion of light by the lattice of contractile proteins," J. Physiol. **290**(2), 317–330 (1979).
4. R. A. Thornhill, N. Thomas, and N. Berovic, "Optical diffraction by well-ordered muscle fibres," Eur. Biophys. J. **20**(2), 87–99 (1991).
5. E. Sidick, A. Knoesen, J. K. Xian, Y. Yeh, and R. J. Baskin, "Rigorous analysis of light diffraction by a striated muscle fibre," Proc. Biol. Sci. **249**(1326), 247–257 (1992).
6. J. Xia, A. Weaver, D. E. Gerrard, and G. Yao, "Monitoring sarcomere structure changes in whole muscle using diffuse light reflectance," J. Biomed. Opt. **11**(4), 040504 (2006).
7. J. Ranasinghesagara, and G. Yao, "Imaging 2D optical diffuse reflectance in skeletal muscle," Opt. Express **15**(7), 3998–4007 (2007).
8. X. Li, J. C. Ranasinghesagara, and G. Yao, "Polarization-sensitive reflectance imaging in skeletal muscle," Opt. Express **16**(13), 9927–9935 (2008).
9. X. Li, and G. Yao, "Mueller matrix decomposition of diffuse reflectance imaging in skeletal muscle," Appl. Opt. **48**(14), 2625–2631 (2009).
10. A. Kienle, F. K. Forster, and R. Hibst, "Anisotropy of light propagation in biological tissue," Opt. Lett. **29**(22), 2617–2619 (2004).
11. A. Kienle, and R. Hibst, "Light guiding in biological tissue due to scattering," Phys. Rev. Lett. **97**(1), 018104 (2006).
12. A. Kienle, C. D'Andrea, F. Foschum, P. Taroni, and A. Pifferi, "Light propagation in dry and wet softwood," Opt. Express **16**(13), 9895–9906 (2008).
13. T. L. Yun, N. Zeng, W. Li, D. Z. Li, X. Y. Jiang, and H. Ma, "Monte Carlo simulation of polarized photon scattering in anisotropic media," Opt. Express **17**(19), 16590–16602 (2009).
14. Z. Nan, J. Xiaoyu, G. Qiang, H. Yonghong, and M. Hui, "Linear polarization difference imaging and its potential applications," Appl. Opt. **48**(35), 6734–6739 (2009).
15. N. Ghosh, H. S. Patel, and P. K. Gupta, "Depolarization of light in tissue phantoms - effect of a distribution in the size of scatterers," Opt. Express **11**(18), 2198–2205 (2003).
16. C. F. Bohren, and D. R. Huffman, *Absorption and Scattering of Light by Small Particles* (John Wiley and Sons, New York, 1983).
17. B. D. Cameron, M. J. Rakovic, M. Mehrübeoglu, G. W. Kattawar, S. Rastegar, L. V. Wang, and G. L. Coté, "Measurement and calculation of the two-dimensional backscattering Mueller matrix of a turbid medium," Opt. Lett. **23**(7), 485–487 (1998).

#126668 - $15.00 USD Received 8 Apr 2010; revised 28 May 2010; accepted 23 Jun 2010; published 30 Jun 2010

1. Introduction

A major goal of biomedical optics studies is to understand the interactions between photons and complicated biological tissues, which usually have to be characterized by simplified models. Skeletal muscle is one of the most abundant tissues in human body and very important for therapeutic and diagnostic applications. It is well understood [1] that skeletal muscle is made up of individual components known as muscle fibers. These fibers are made from myofibrils which are long cylinders of about 1-2μm diameter. The term muscle refers to multiple bundles of muscle fibers held together by connective tissue. The gap among the myofibrils is full of sarcoplasma consisting of cellular organelles. Since the myofibrils of skeletal muscle consist of periodic sarcomeres with different refractive index [2], people usually treated a single myofibril as an optical phase grating [3] and used a coupled-wave theory to calculate the coherent interaction between incoming beam and a single myofibril or well-ordered bundle [4–9]. On the other hand, since skeletal muscle is highly turbid in optical region, scattering effects have to be considered in many optical measurements. It is necessary to characterize the optical property of skeletal muscle using a proper scattering model. In earlier publications, well aligned infinitely long cylinders [10,11] or a mixture of aligned cylinders and isotropic scatterers [12] have been used to simulate unpolarized photon propagation in anisotropic turbid media such as dentin and softwood, even porcine artery. Recently, we developed a polarization-dependent Monte Carlo program for simulating polarized photon propagation in scattering media containing only solid spheres and infinitely long cylinders [13]. We also used the program and the sphere-cylinder scattering model (SCSM) to explain the behavior of linear polarization difference (LPD) and anisotropy parameter G in rotating linear polarization imaging (RLPI) of different biological tissues, including skeletal muscle [14]. In this paper, we demonstrate, using both experiments and Monte Carlo simulations, that SCSM can reproduce all the characteristic features in spatially resolved unpolarized, polarized reflectance and Mueller matrix elements of skeletal muscle. The evidences indicate that SCSM may be used to characterize both the anisotropic optical properties (i.e. parameters of the scatterers and the ambient medium), and the anisotropic structure (i.e. alignment of the fibers) of skeletal muscle.

2. Material and method

In this paper, we use a microsphere-silk sample as the phantom to the SCSM. The sample consists of a slab of well aligned silk fibers submerged in microsphere solution as shown in Fig. 1. It contains three layers, and the thickness of the first and third layers is adjustable. In previous studies of isotropic tissue phantoms, it is found that the depolarization characteristics of tissues are mainly affected by small scatterers [15]. Therefore, the first and third layers are solutions of 0.2μm diameter polystyrene microsphere in water (International Laboratory, USA) as an equivalent approximation of the cellular organelles. The refractive indices of the microsphere and water are 1.59 and 1.33 respectively, and the scattering coefficient is selected as $5cm^{-1}$ for experimental convenience. It is smaller than the scattering coefficients of most biological tissues, but allows us to vary the thickness of the first layer in a wider range for better qualitative measurement results. This choice does not change our conclusion. The second layer contains only well aligned silk fibers (provided by Guangxi Institute of Supervision and Testing on Product Quality). Its thickness is 3mm and refractive index is 1.56. We have measured the diameter of silk fiber using a SEM. Since silk fiber contains substructure, its diameter is taken as 1.5μm. By comparing simulated and experimental results, we estimated that the scattering coefficient of silk layer is $70cm^{-1}$ [13]. In experiments, the sample surface is set as the X-Y plane, the fibers are aligned in the plane and parallel to the y-axis (the vertical direction of the image). During experiments, the depth of submersion can be adjusted to vary the ratio of scattering coefficients between spheres and cylinders. As the depth of submersion increases, thickness of the first layer increases. Photons interact with more spheres before reaching the well aligned silk fibers, which corresponds to

#126668 - $15.00 USD Received 8 Apr 2010; revised 28 May 2010; accepted 23 Jun 2010; published 30 Jun 2010

an increase in the ratio of scattering coefficients between spheres and cylinders. In this paper, thickness of the first layer is 1mm for an optimum match to the results of skeletal muscle.

Although such a separately spaced sphere-cylinder sample is different from a true SCSM in which spheres and cylinders are mixed together, it will be shown later in this article that such layered microsphere-silk sample generates very similar results as the homogeneous sphere-cylinder scattering medium. Monte Carlo simulations indicate that the two display very similar characteristic features.

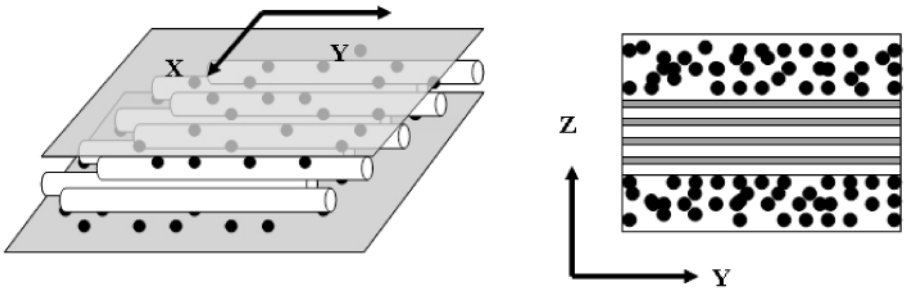

Fig. 1. Schematics of the three-layer microsphere-silk sample. The first and third layers are 0.2μm diameter polystyrene microsphere in water. The second layer is 1.5μm diameter well aligned silk fibers in water. Total thickness of the sample is 2cm. Thickness of the first and third layers is adjustable, and of the second layer is 3mm.

The SCSM for our polarization-dependent Monte Carlo simulation has been reported previously [13] and is summarized as follow. The SCSM consists of two types of scatterers: solid spheres and infinitely long cylinders. The angular distribution of the cylinders follows a Gaussian distribution. Variables of SCSM include parameters of the scatterers and the surrounding medium. Those for the scatterers are numbers of spherical and cylindrical components, their number densities and sizes, the mean value and standard deviation of the direction distribution function for the cylinders. Those for the surrounding medium are birefringence, dichroism, refractive index and absorption coefficient which may or may not be polarization dependent. In this letter, we use the simplest SCSM which contains only single dispersed spheres and cylinders immersed in isotropic liquid of zero absorbance. In Monte Carlo simulations, by solving the scalar wave equation analytically, we can pre-calculate the Mueller matrix of infinitely long cylinder [16]. The program starts with launching the normal incident photon whose polarization state is represented by a Stokes vector. At each scattering event, we make a statistical choice on what type of scatterer the photon hits. Then the program rotates the Stokes vector reference frame and computes the phase function using the pre-calculated scattering matrices. The scattering direction is determined according to the phase function together with a random number and then the Stokes vector is updated. The simulation process continued until a photon is completely absorbed or move out of the sample. Locations, polarization states and other information of the emitted photons are stored.

#126668 - $15.00 USD Received 8 Apr 2010; revised 28 May 2010; accepted 23 Jun 2010; published 30 Jun 2010

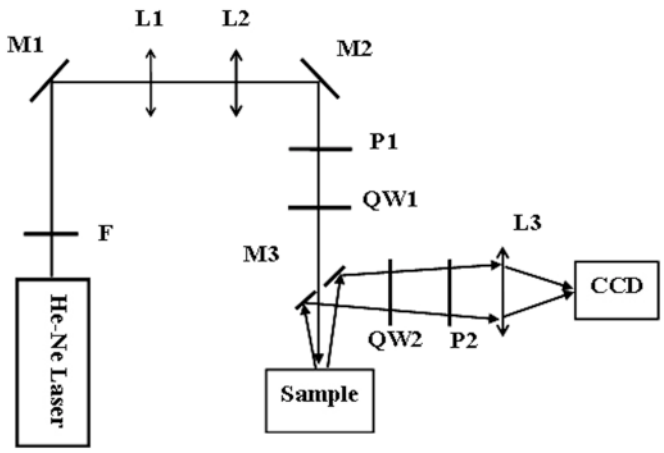

Fig. 2. A schematic of the experimental setup. F: filter; M: mirror; L: lens; P: polarizer; QW: quarter wave plate.

The experimental set up adopts a typical configuration for Mueller matrix measurements [8] as shown in Fig. 2. A 12mW linearly polarized He-Ne laser (China Daheng Optics DH-HN600) at 633nm is the light source. A quarter-wave plate and a linear polarizer are used to control the incident polarization. A front surface mirror titled at a 45 degree angle to the normal is positioned in front of the sample. A piece of cover glass is place on top of the sample to ensure a flat imaging surface. The incident light reaches the sample through a 5mm hole at the center of the mirror. Reflection from the flattened sample surface passes through the same hole and is eliminated. Backscattered photons are steered to and recorded by a 14-bit CCD camera (Canon APS-C) to produce spatially resolved reflectance images. A second set of quarter-wave plate and linear polarizer in front of the CCD controls the reflectance polarization. Fresh bovine *Sternomandibularis* muscle samples used in this study were excised from animals 2 hours after slaughtering. However, time interval between slaughtering and the actual measurements may vary between 2 to 3 hours.

$$M = \begin{pmatrix} M_{11} & M_{12} & M_{13} \\ M_{21} & M_{22} & M_{23} \\ M_{31} & M_{32} & M_{33} \end{pmatrix} = \frac{1}{2}\begin{pmatrix} HH+HV+VH+VV & HH+HV-VH-VV & 2PH+2PV-M_{11} \\ HH-HV+VH-VV & HH-HV-VH+VV & 2PH-2PV-M_{21} \\ 2HP+2VP-M_{11} & 2HP-2VP-M_{12} & 4PP-2PH-2PV-M_{31} \end{pmatrix} \quad (1)$$

In this paper, to determine the 3 × 3 Mueller matrix, we take three different polarization states for the incident light-horizontal linear (H), vertical linear (V), 45 linear (P), and measure three polarization components of the optical reflectance corresponding to each incident polarization. The rest of Mueller matrix elements related to circular polarization are not considered since they do not show clear patterns [9]. The Mueller matrix can be calculated as Eq. (1), where the first capital letter represents the input polarization state, and the second letter represents the output polarization state. It is shown in Eq. (1) that M11 corresponds to unpolarized reflectance. A total of 9 reflectance images are captured in the experiment. Using these reflectance images, we can get the equi-intensity profile (EIP) and Mueller matrix of the skeletal muscle and microsphere-silk sample.

3. Results and discussion

We first compare the experimentally observed unpolarized reflectance images of skeletal muscle and sphere-cylinder sample as shown in Fig. 3. For both samples, the fibrous

#126668 - $15.00 USD Received 8 Apr 2010; revised 28 May 2010; accepted 23 Jun 2010; published 30 Jun 2010

structures are oriented along the vertical direction, or the y-axis. The equi-intensity profile (EIP) of reflectance images of the skeletal muscle (Fig. 3a) takes a distinctive rhombus shape as reported by another group [7]. Both experiments with variable ratio microsphere-silk sample and Monte Carlo simulations with SCSM show that EIP becomes circular or elliptical if the sample contains only spheres (Fig. 3c) or cylinders. EIP becomes rhombic when the sample contains both types of scatterers (Fig. 3b). This is because photons tend to be scattered to the perpendicular direction of cylindrical scatterers [16], i.e. the x-axis in this paper. Therefore the unpolarized reflectance EIP of skeletal muscle can be considered as a combination of the contributions of both spherical and cylindrical scatterers. The rhombic EIP becomes increasingly circular for higher sphere-cylinder ratio. In the experiments, by varying the depth of submersion of the silk slab, we find a sphere-cylinder ratio which gives the best fit between the experimental results of microsphere-silk sample (Fig. 3b) and skeletal muscle (Fig. 3a). Despite the apparently different microstructure of the two samples, the two images demonstrate the same characteristic features. Therefore for the study of unpolarized optical properties, such as the relative concentration of cylinders and scattering coefficient, of bulk skeletal muscle, SCSM is a feasible model.

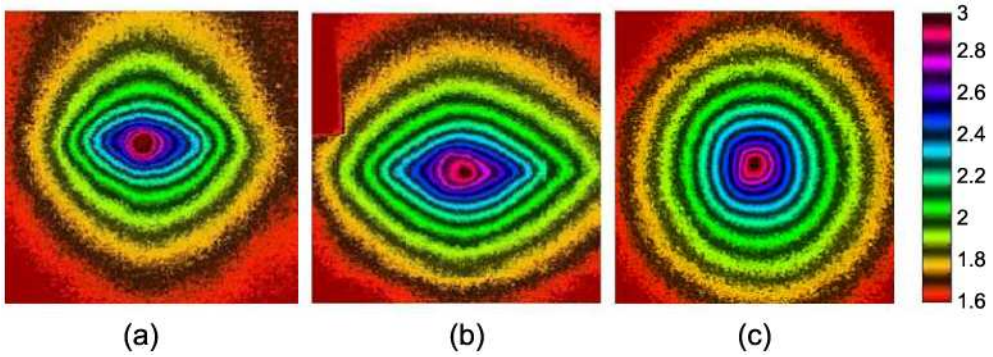

Fig. 3. The reflectance images of (a) fresh skeletal muscle, (b) microsphere-silk sample; (c) 0.2μm diameter polystyrene microsphere solution. Images were displayed in pseudo color which represented the pixel intensity in 10-based Logarithm. The artifact on the upper left corner of (b) is due to a clip which holds the fibers.

We then keep the same experimental condition and compare the polarized reflectance images and Mueller matrix elements of the skeletal muscle and the microsphere-silk sample, which provide more sensitive tests of SCSM. For polarized reflectance, a total of 9 EIP images are displayed corresponding to different combinations of incidence and reflectance polarization states, i.e. horizontal linear (H), vertical linear (V), and 45 degree linear (P).

Figure 4. shows the polarized reflectance EIP images of the very crude microsphere-silk sample (Fig. 4b) containing the same characteristic features of skeletal muscle (Fig. 4a) [8,9]. Among 9 EIP images, HH, HP, PH and PP are rhombic, while the shapes of the other five lie between rhombus and ellipse. The VV image, which corresponds to vertical incident polarization and vertical reflectance polarization states, has the highest intensity and is elongated along x-axis. The HH image shows a distinct rhombus shape of more balanced intensities along x-axis and y-axis. The EIP of other images have patterns that lie between HH and VV. Moreover, all images have a diagonal symmetric relationship. For instance, HV and VH are similar. It should be pointed out that the polarized reflectance images for skeletal muscle and microsphere-silk sample do not match quantitatively. This is due to the different absorption and scattering coefficients of the two samples. Monte Carlo simulation with SCSM indicates that if we increase the total scattering coefficient while keeping the ratio between scattering coefficients of the two types of scatterers constant, the shapes of EIP images stay the same but their sizes decrease.

#126668 - $15.00 USD Received 8 Apr 2010; revised 28 May 2010; accepted 23 Jun 2010; published 30 Jun 2010

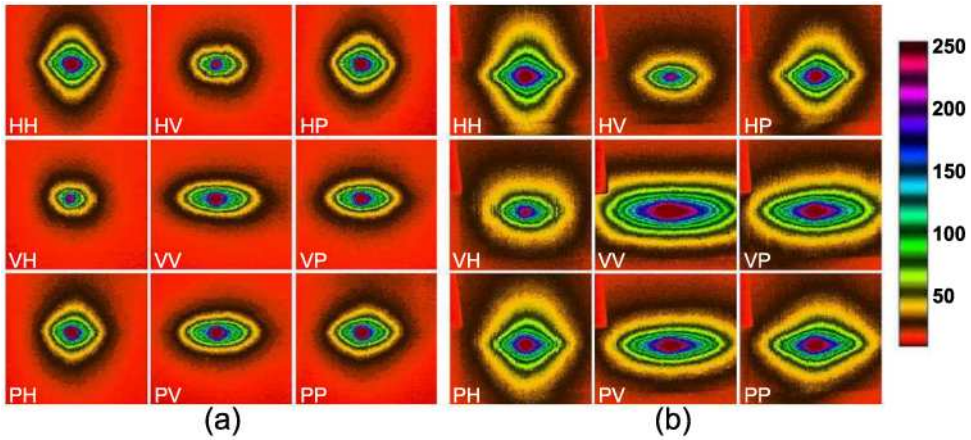

Fig. 4. Polarized reflectance images of (a) fresh skeletal muscle and (b) microsphere-silk sample. The image size is 1.4cm × 1.27cm. The muscle fibers and silk fibers are along the vertical direction.

The differences in "VV" and "HH" images can be explained using Mie scattering theory for spheres and infinitely long cylinders [16]. Polarization maintaining photons tend to be scattered to the perpendicular direction of cylindrical scatterers, i.e. the x-axis in this paper. For horizontal and vertical incident polarization, photons scattered along x-axis are more likely to be in H and V polarization state, respectively. However, for a sphere-only medium, the EIP images are quite different as shown in Fig. 5a and Fig. 5b. The polarized reflectance EIP images of skeletal muscle can be considered as a combination of the contributions of both spherical and cylindrical scatterers. Hence, compared to sphere-only medium, all 9 reflectance EIP images of microsphere-silk sample are elongated along x-axis due to the scattering of cylinders. So the intensity at x-axis is much higher than at y-axis for VV image, while for HH image, the intensity at x-axis is slightly higher than that at y-axis. In order to explain the elongation effect quantitatively, we compare the axis lengths along the x and y directions of different samples. The value of x/y represents the ratio of the axis lengths along the x and y directions. HH image is normalized by the maximum intensity Imax. Figure 5c shows the dependence of x/y to normalized intensity I/Imax for HH images. As normalized intensity increases from 0.1 to 0.5, x/y values for both skeletal muscle and microsphere-silk samples increase from ~0.9 to ~1.4; then normalized intensity increases from 0.5 to 0.9, x/y values for both samples decrease to 1. However, for sphere-only sample, as normalized intensity increases from 0.1 to 0.9, x/y value monotonically increases from 0.5 to 1, which is very different from x/y values for both skeletal muscle and microsphere-silk sample. Moreover, x/y values for skeletal muscle and microsphere-silk sample are higher than those for sphere-only sample. The higher x/y values show an elongation effect along x-axis.

#126668 - $15.00 USD Received 8 Apr 2010; revised 28 May 2010; accepted 23 Jun 2010; published 30 Jun 2010

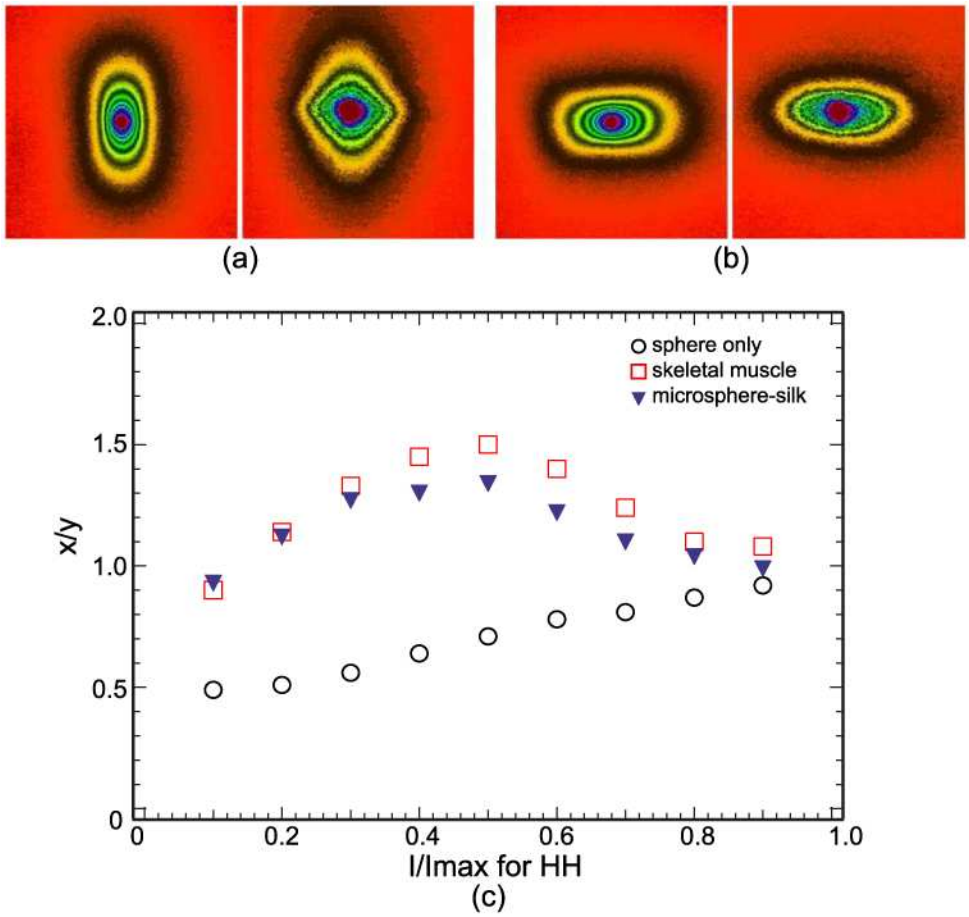

Fig. 5. (a) from left to right: HH for sphere-only medium; HH for skeletal muscle, (b) from left to right: VV for sphere-only medium; VV for skeletal muscle, (c) comparison of the HH images of different samples, dependence of x/y to the normalized intensity.

Such effects due to the cylindrical scatterers also explain the characteristic features of skeletal muscles in Mueller matrix elements [8]. As shown in. Figure 6, the experimental results of the microsphere-silk sample (Fig. 6b) and skeletal muscle (Fig. 6a) agree to each other qualitatively. M11 for muscle has typical rhombus shape. Due to the existence of spherical scatterers, M12 and M21 elements for both the skeletal muscle and the microsphere-silk sample are quatrefoils, i.e. intensity is negative around x-axis and positive around y-axis, which are similar to intensity distribution in a sphere-only medium [17]. Closer observations reveal that intensity around x-axis is much higher than that around y-axis, this is because polarization maintaining photons tend to be scattered along the x-axis. The difference becomes even bigger when the concentration of cylindrical scatterers increases. Increasing the sphere-cylinder ratio reduces the intensity ratio between x-axis and y-axis. For the same reason, M22 element's intensity along x-axis is dominant while that along y-axis is very weak. Other elements have no typical patterns in the images obtained from both skeletal muscle and microsphere-silk sample.

#126668 - $15.00 USD Received 8 Apr 2010; revised 28 May 2010; accepted 23 Jun 2010; published 30 Jun 2010

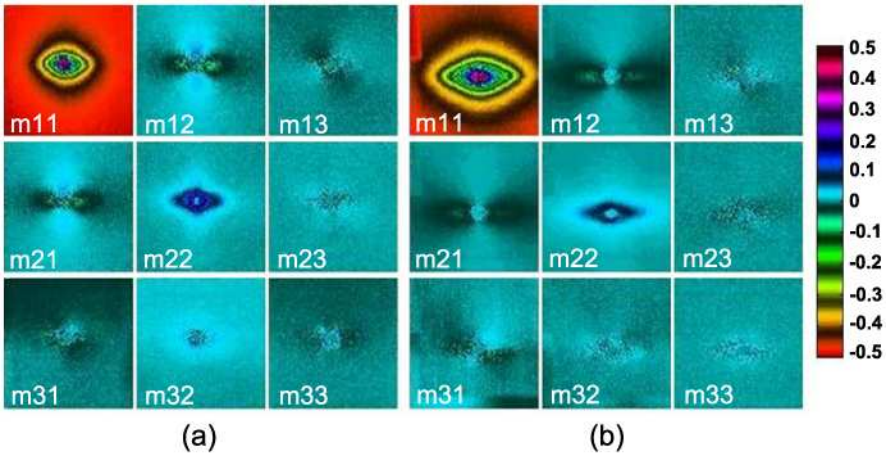

Fig. 6. The Mueller matrix images in (a) fresh skeletal muscle and (b) microsphere-silk sample. The image size is 1.4cm × 1.27cm. The muscle fibers and silk fibers are along the vertical direction (y-axis).

We are also able to obtain quantitative agreement between Monte Carlo simulations with SCSM and the experimentally observed polarized reflectance images of skeletal muscle. Here we take M22 as an example (Fig. 7). In simulations, the solid spheres and infinitely long cylinders represent the cellular organelles and myofibrils respectively. Their diameters are 0.4μm and 1.5μm and their refractive indices are 1.4, all of which are close to the quoted parameters of skeletal muscle [1]. The refractive index of surrounding medium is taken as 1.33. The standard deviation of angular distribution of the cylinders is 10 degree. Ratio between the scattering coefficients of microspheres and cylinders at normal incidence is set at 10/40 to give the best match in the shape of the images. The total scattering coefficient in the simulation is then altered until the simulated EIP image matches the experimental one, as shown in Fig. 7. The total scattering coefficient along the y-axis corresponding to the best fit is 50 ± 10cm^{-1}, which is close to the scattering coefficient of skeletal muscle [7]. Figure 7. shows that both the three-layer and homogeneous Monte Carlo simulated results agree quantitatively with experimental results of skeletal muscle. The M22 is elongated to x-axis due to the scattering of cylinders. For the equi-intensity contour of 0.05, the x/y values for skeletal muscle, three-layer Monte Carlo simulation and homogeneous Monte Carlo simulation are 1.73, 1.71 and 1.70, respectively. The simulated images match the experimental one except around the center where CCD saturates.

In fact, a closer examination of the simulated results reveals that different elements of the spatially resolved polarized reflectance (Fig. 4) or the Mueller matrix (Fig. 6) have different response to changes in SCSM parameters. The characteristic features in these images can be exploited to obtain a unique set of SCSM parameters which characterize the structural and optical properties of skeletal muscle.

#126668 - $15.00 USD Received 8 Apr 2010; revised 28 May 2010; accepted 23 Jun 2010; published 30 Jun 2010

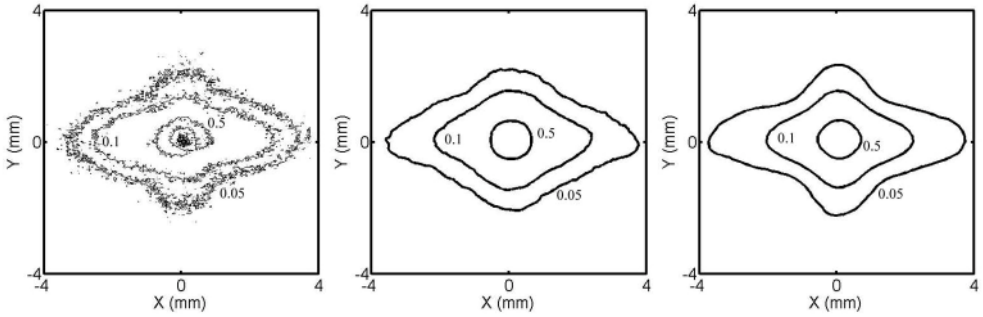

Fig. 7. From left to right: The contour of M22 from fresh skeletal muscle and; three-layer Monte Carlo simulation; homogeneous Monte Carlo simulation. The image size is 0.8cm × 0.8cm. The muscle fibers are along the vertical direction (y-axis).

4. Conclusion

In summary, we have measured the unpolarized and polarized reflectance as well as Mueller matrix elements of both skeletal muscle and a simple sphere-cylinder scattering medium, which consists of only polystyrene microspheres and silk fibers. Despite the apparent difference in the microstructure and optical properties of the two samples, the characteristic features in the experimental results are very similar. Polarization sensitive Monte Carlo simulation has also demonstrated that the simple sphere-cylinder scattering model is capable of generating a quantitative match to the experimental result of skeletal muscle. These evidences prove that SCSM may be used to characterize the structural and optical properties of bulk skeletal muscle potentially. In addition, the characteristic features of SCSM and how parameters of SCSM affect these features should be explored. Since most biological tissues are optically turbid and many of them contain microstructure of ordered elongated subunits, SCSM is expected to be a general model for tissue optics and a useful tool for the studies of the complicated interactions between polarized photons and fibrous biological tissues.

Acknowledgement

This work is supported by National Natural Science Foundation of China (grant 60778044, 30770592, 60608019 and 10974114) and Ministry of Science and Technology (973 Program No. 2006CB70570).

#126668 - $15.00 USD Received 8 Apr 2010; revised 28 May 2010; accepted 23 Jun 2010; published 30 Jun 2010